THE JOURNAL OF PHYSICAL CHEMISTRY C

Article

pubs.acs.org/JPCC

Enhanced Bulk Thermoelectric Performance of $Pb_{0.6}Sn_{0.4}Te$: Effect of Magnesium Doping

Sandhya Shenoy and D. Krishna Bhat*

Department of Chemistry, National Institute of Technology Karnataka, Surathkal Srinivasnagar, Mangalore, 575025, India

Supporting Information

ABSTRACT: Thermoelectric (TE) materials are promising in the context of renewable power generation as they can directly convert waste heat into electricity. Although PbTe is the best known TE material, its use is not encouraged due to concerns of environmental toxicity of lead. A combination of modified self-propagating high-temperature synthesis (SHS) and field-assisted sintering technique (FAST) is employed for the very first time to synthesize a solid solution of PbTe and SnTe. We show that doping of $Pb_{0.6}Sn_{0.4}Te$ with Mg breaks crystal mirror symmetry and opens up band gap. This results in suppression of bipolar diffusion. Also the increase in degeneracy of valence sub-bands improves Seebeck coefficient. Both these synergistically leads to remarkable enhancement in figure of merit ZT (~2 at 840 K) and ZT_{avg} (~1.2 between 500 and 840 K) rendering it into high-performance thermoelectric material by successfully engineering electronic structure. Most importantly, the ZT here is comparable to that of Mg-doped PbTe but has lesser lead content and hence is more environment friendly. The most probable configuration of $Pb_{0.6}Sn_{0.4}Te$ was also determined for the very first time using site occupancy disorder (SOD) technique.

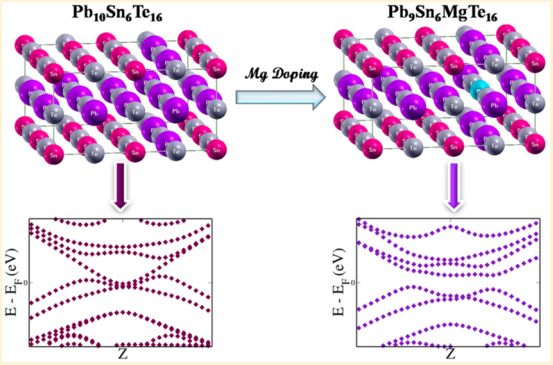

INTRODUCTION

The ever-increasing demands of energy and exhaustion of nonrenewable fossil fuel resources at an alarming rate caused by its abuse has triggered the attention of scientific community to consider all options of renewable power generation. Thermoelectric (TE) materials are a class of materials which have the ability to directly and reversibly convert temperature difference into electric potential. They can in fact tap very well the vast resources of mostly underutilized thermal energy and can contribute to solve the ever increasing energy crisis.[1,2] While all materials have a non-zero thermoelectric effect, in most materials it is too small to be useful. Hence obviously, identifying materials with higher thermoelectric efficiency than available at present is need of the day. This is a challenge due to the conflicting combination of material traits expected. The well-known interdependence of Seebeck coefficient (S), electrical conductivity (σ), and thermal conductivity (κ) complicates efforts to develop strategies for improving a material's average figure of merit ZT (where $ZT = \sigma S^2 T/\kappa$).[1,2] In search of new materials with higher efficiency and in an attempt to improve the efficiency of already known materials, solid solutions of PbTe and SnTe have been studied. One such class, $Pb_xSn_{1-x}Te$, is found to be topological crystalline insulator where topological protection is ensured by crystalline symmetry instead of time reversal symmetry.[3−6] The electronic structure of $Pb_xSn_{1-x}Te$ has been altered by breaking the crystal symmetry using techniques like applying electric field, mechanical straining, and ferroelectric structural distortion and engineering the thickness of the material,[6−9] but most of these are physical perturbations. Engineering the electronic structure of $Pb_xSn_{1-x}Te$ by chemical doping is rarely reported.[10,11]

PbTe and its alloys are the best known TE materials,[12−18] but due to the toxic effects of lead, use of PbTe-based materials is limited. SnTe, a homologue of PbTe, has similar rock salt structure and electronic structure. It is considered safe but suffers from low ZT due to smaller band gap and higher separation between the valence sub-bands.[19] Hence, developing environment friendly materials with higher thermoelectric efficiency than available at present is of utmost importance in the current global scenario. $Pb_{0.6}Sn_{0.4}Te$ is a well-known TCI derived from PbTe and SnTe. Compared to PbTe, this is a better material as far as environmental toxicity is considered, but it has a negligible band gap which makes its thermoelectric properties very poor. However, it was recently reported that doping with group I metals (Na and K) improves the overall thermoelectric performance of $Pb_{0.6}Sn_{0.4}Te$, but the figure of merit achieved was ~1 which shows that there is a large scope for improvement.[10,11]

We thought it is worth investigating the effect of doping $Pb_{0.6}Sn_{0.4}Te$ with divalent group II metals. Accordingly, we report here the effect of Mg doping on the electronic structure

Received: July 17, 2017
Revised: September 1, 2017
Published: September 5, 2017

DOI: 10.1021/acs.jpcc.7b07017
J. Phys. Chem. C 2017, 121, 20696−20703

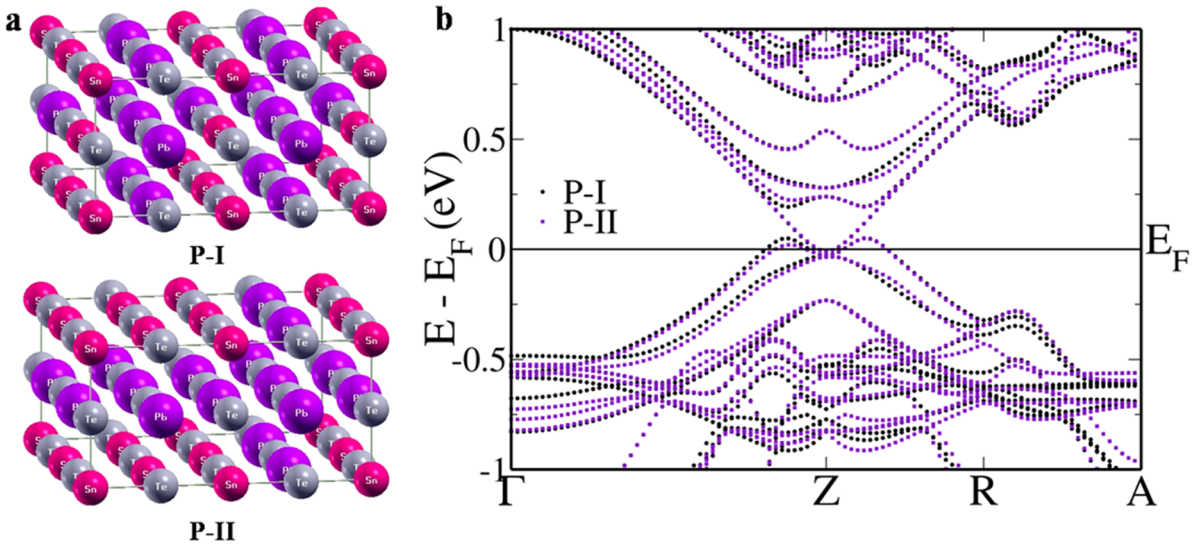

Figure 1. (a) Crystal structures P-I and P-II showing the most stable configurations of $Pb_{10}Sn_6Te_{16}$. (b) Electronic structures of P-I (black) and P-II (purple) configurations of $Pb_{0.6}Sn_{0.4}Te$ simulated using a 2 × 2 × 1 supercell.

and thermoelectric properties of $Pb_{0.6}Sn_{0.4}Te$ employing first-principles calculations. Most importantly, we also determined the most probable configuration of $Pb_{0.6}Sn_{0.4}Te$ for the very first time using site occupancy disorder (SOD) technique.[20] In light of the theoretical predictions, synthesis of the material was carried out, and its properties were determined. A combination of modified self-propagating high-temperature synthesis (SHS) and field-assisted sintering technique (FAST) is employed for the synthesis. The theoretical results confirmed by experiments show that Mg breaks the crystal mirror symmetry of $Pb_{0.6}Sn_{0.4}Te$ and opens up the band gap which causes the suppression of thermal conduction due to bipolar diffusion. Alloying Mg with $Pb_{0.6}Sn_{0.4}Te$ decreases the energy separation between light and heavy hole valence sub-bands and hence increases the contribution of the latter leading to improvement in the Seebeck coefficient. These effects put together cause remarkable improvement in the ZT (∼2 at 840 K) of the Mg-alloyed $Pb_{0.6}Sn_{0.4}Te$.

METHODS

Computational Details. The electronic structure of pristine and Mg-alloyed $Pb_{10}Sn_6Te_{16}$ were determined by density functional theoretical (DFT) calculations using Quantum Espresso package.[21] To account for the effect of spin orbit coupling, relativistic effect cannot be neglected during the elucidation of realistic electronic structure. Since Pb, Sn, and Te have high atomic numbers, fully relativistic ultrasoft pseudopotentials were used for the calculations. $5d^{10}6s^26p^2$, $4d^{10}5s^25p^2$, $4d^{10}5s^25p^4$, and $3s^2$ were considered as valence electrons of Pb, Sn, Te, and Mg respectively and included in the calculations through the use of pseudopotentials. The exchange-correlation energy functional was approximated with a Generalized Gradient Approximation (GGA) with parametrized functional of Perdew, Burke, and Erzenhoff (PBE).[22] PbTe and SnTe crystallize in the rocksalt structure with two atoms per unit cell and *Fm3m* space group symmetry. To simulate substitutional doping, a 2 × 2 × 1 supercell containing 32 atoms were used. A 10 × 10 × 20 uniform grid of k-points was used to sample integrations over the Brillouin-zone of the supercell. An energy cutoff of 50 Ry and charge density cutoff of 400 Ry was used to truncate the plane wave basis representing wave functions. The discontinuity in occupation numbers of electronic states was smeared using Gaussian smearing with a width of 0.01 eV. Electronic structure of $Pb_9Sn_6MgTe_{16}$ (∼6.25% Mg-doped) was determined along high symmetry lines (Γ−Z−R−A) in the Brillouin zone.

Synthesis. High-purity (+99.99%) tin, tellurium, lead, and magnesium were procured from Alfa Aesar and were used for synthesis without further purification. High-quality crystalline ingots of $Pb_{0.6-x}Sn_{0.4}Mg_xTe$ (x = 0.0, 0.02, 0.04, 0.06, and 0.08) were synthesized by mixing high-purity Sn, Te, Pb, and Mg in appropriate ratios using a mortar and pestle. The mixture was then cold-pressed into a pellet in a dye under 5 MPa pressure. The pellet was then sealed under vacuum (10^{-5} Torr) in carbon-coated quartz tube. The pellet was ignited using a hand torch to initiate SHS process. The combustion wave passed through the pellet within seconds. The thus-obtained product was again ground using mortar and pestle and was later densified using FAST technique (SPS-211LX, Fuji Electronic Industrial Co., Ltd.) at 773 K in a graphite dye in vacuum. The resulting sample was further subjected to annealing treatment at 1173 K for 24 h.

X-ray Diffraction. Powder X-ray diffraction (pXRD) of all the samples were recorded on Bruker D8 diffractometer using a Cu Kα (λ = 1.5406 Å) radiation.

Band Gap Measurement. Finely ground sample was used to measure the optical band gap at room temperature using FTIR Bruker IFS 66 V/S spectrometer with 2 cm^{-1} resolution and 50 scans. Kubelka−Munk equations were used to calculate absorption data from the reflectance data. The energy band gaps were derived from absorption versus energy (in eV) plot.

Transport Properties. ULVAC-RIKO ZEM-3 instrument system was used to determine electrical conductivity and Seebeck coefficient from 300 to 840 K under helium atmosphere. The sample was cut in parallelepiped shape with dimensions ∼2 × 2 × 8 mm^3 and the thermal conductivity was measured in the longer direction. Carrier concentrations were determined with a PPMS system using Hall coefficient measurements at 300 K using four-contact Hall-bar geometry. The carrier concentration, n, was estimated from the formula: $n = (eR_H)^{-1}$, where e is the electronic charge. Thermal diffusivity was measured using laser flash diffusivity method in a Netzsch

DOI: 10.1021/acs.jpcc.7b07017
J. Phys. Chem. C 2017, 121, 20696−20703

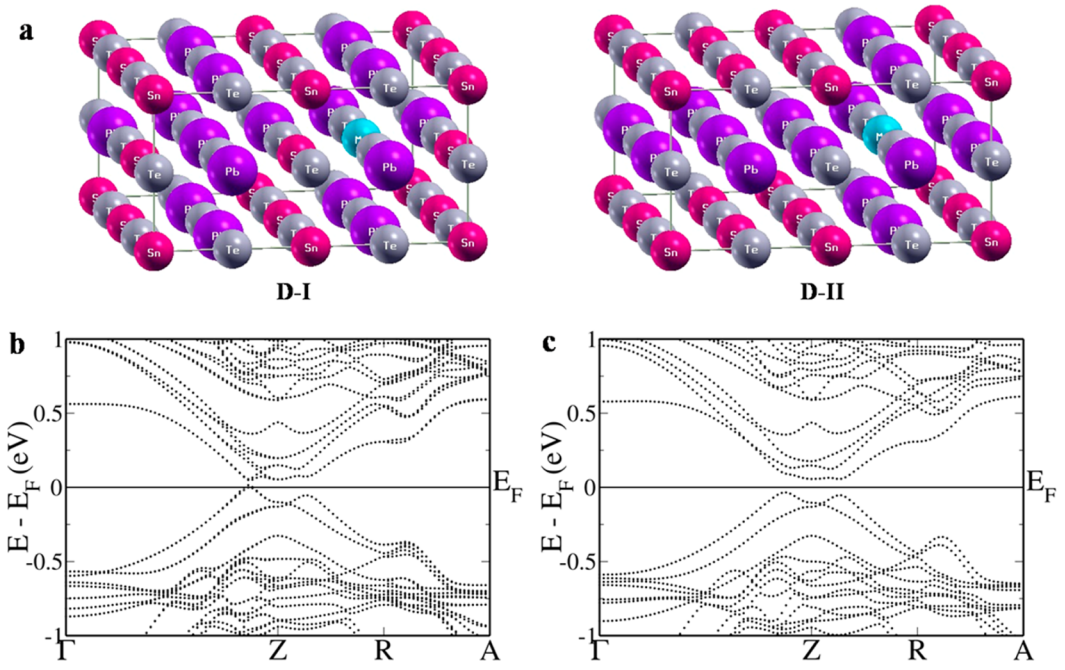

Figure 2. (a) Crystal structures of $Pb_9Sn_6MgTe_{16}$ with D-I and D-II configurations with Mg in rock salt site substituted for Pb. Electronic structures of $Pb_9Sn_6MgTe_{16}$ with (b) D-I and (c) D-II configurations determined using first-principles calculations showing the opening up of band gap.

LFA-457 in the temperature range from 300 to 840 K. The sample was cut in the shape of coins with ∼8 mm diameter and ∼2 mm thickness. The total thermal conductivity was calculated using the formula, $\kappa_{total} = DC_p\rho$, where D is thermal diffusivity, C_p is temperature-dependent heat capacity (derived using standard sample (pyroceram) in LFA-457), and ρ is the density of the sample, measured using the sample dimension and mass.

RESULTS AND DISCUSSION

$Pb_{0.6}Sn_{0.4}Te$, a TCI with almost zero band gap, possesses very poor thermoelectric properties. However, recently it is reported that Na and K doping in $Pb_{0.6}Sn_{0.4}Te$ improves its overall thermoelectric performance.[10,11] It is also understood that a solid solution alloying of MgTe has significant effect on the thermoelectric properties of both PbTe as well as SnTe.[12−14,23] In view of these facts, first-principles analysis of electronic structure of Mg alloyed $Pb_{0.6}Sn_{0.4}Te$ was carried out. Experimental verification of theoretical output was done by synthesis of the material and study of its properties.

To simulate $Pb_{0.6}Sn_{0.4}Te$, a 2 × 2 × 1 supercell was constructed containing 32 atoms, based on the rock salt structure of parent PbTe and SnTe. However, it may be noted that the determination of most probable structure here is complicated due to the innumerable probabilities that exist for occupation of Sn and Mg atoms at the Pb atom sites of the host structure leading to several configuration of chemical ordering. In earlier reports on $Pb_{0.6}Sn_{0.4}Te$, the configuration was randomly chosen for simulation.[10,11] Recently, we have shown that the site occupied by the atom in a crystal has immense effect on its electronic structure and properties.[24] Hence, we employed the SOD technique to determine the symmetry inequivalent configurations in the supercell.[20] The SOD technique, which is used to model site-disordered solids, takes advantage of crystal symmetry of the lattice to reduce the number of site-occupancy configurations. In $Pb_{10}Sn_6Te_{16}$ supercell, there are 8008 configurations corresponding to the occupation of Sn at Pb sites. SOD technique reduces them to 101 symmetry-inequivalent configurations. The total energies of all the 101 configurations were determined. It was found that two of the configurations (labeled P-I and P-II in Figure 1a) had similar energies and were also the lowest energy states. The electronic structures (Figure 1b) of these two configurations revealed that the band gap of $Pb_{10}Sn_6Te_{16}$ is nearly zero consistent with the earlier reports.[10,11] The valence band maxima and the conduction band minima occurring at L point and the heavy hole valence band occurring at Σ point in the Brillouin zone of the rock salt structure of PbTe/SnTe fold on to Z point and R+Δ point, respectively in the present 2 × 2 × 1 supercell calculation due to periodicity of the reciprocal space. The electronic structures of P-I and P-II configurations are similar with valence band peaking slightly away from the Z point giving it a holelike character, and the conduction band touching the Fermi level giving it an electron-like character.[10,11]

As it is known that breaking of the inversion symmetry leads to opening of band gap, Mg-doped $Pb_{10}Sn_6Te_{16}$ was simulated in such a way that substitution of Mg breaks the inversion symmetry of the crystal in the case of both P-1 and P-II configurations (doped samples denoted as D-I and D-II in the case of P-I and P-II, respectively; Figure 2a).[10,11] Electronic structure of $Pb_9Sn_6MgTe_{16}$ (Figure 2b,c) reveals that incorporation of Mg into the pristine sample opens up the band gap as expected. Visualization of wave functions at Z point reveals that though the contribution of Mg states are seen in higher energy conduction bands the presence of Mg causes reshuffling and mixing of states causing the band gap to open up. While the contribution of Te (p) orbitals to the valence band is undisturbed, the contribution of p orbitals of Pb and Sn atoms to the conduction band are reversed, in agreement with the previous report.[10,11] The electronic structure of D-I configuration shows uneven opening up of the band gap with values of ∼0.035, ∼0.154, and ∼0.128 eV at Z − δ, Z, and Z + δ' points, respectively, in the Brillouin zone. This observation is similar to the pattern obtained in the case of Na and K doping

DOI: 10.1021/acs.jpcc.7b07017
J. Phys. Chem. C 2017, 121, 20696−20703

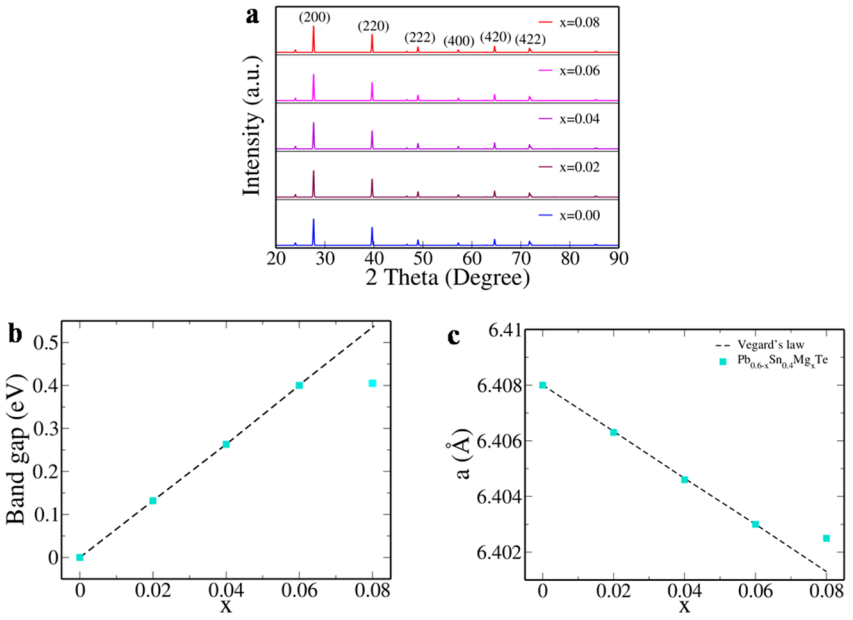

Figure 3. (a) pXRD pattern of $Pb_{0.6-x}Sn_{0.4}Mg_xTe$. Variation of (b) band gap and (c) lattice parameter with concentration of Mg in $Pb_{0.6-x}Sn_{0.4}Mg_xTe$.

of $Pb_{0.6}Sn_{0.4}Te$.[10,11] In contrast, for D-II configuration, the extent of band gap opening is slightly higher. The values are ∼0.126, ∼0.157, and ∼0.111 eV at Z − δ, Z, and Z + δ' points in the Brillouin zone, respectively. Since this coincides with the experimental increase in the band gap discussed in later section, it may be safely assumed that the crystal structure of the sample corresponds to the D-II configuration keeping in mind the typical underestimation of band gap by DFT calculations.

In addition to the opening up of the band gap, introduction of Mg into $Pb_{10}Sn_6Te_{16}$ causes the convergence of light hole and heavy hole valence sub-bands (see Figures 1 and 2) as in the case of parent material PbTe and SnTe.[12,23] The energy difference between the two valence sub-bands decreases from ∼0.331 to ∼0.280 eV for ∼6 mol % doping of Mg (D-II configuration) as opposed to a decrease of ∼0.375 to ∼0.370 eV in the case of Mg-doped SnTe for the same concentration of doping.[23] Since MgTe is known to crystallize in zinc blende structure in addition to rock salt structure, Mg was substituted in zinc blende site in D-II configuration, and simulation was carried out. Even in this case we see that the band gap opens up to about ∼0.063 eV at Z − δ and Z + δ' points and ∼0.1 eV at Z point in the Brillouin zone. The energy difference between the light and heavy hole valence bands drastically reduces to ∼0.231 eV (Figure S1). This convergence results in increase in the density of states asymmetrically near the Fermi level. Thus, an increase in the degeneracy of the valence bands makes both the bands to contribute toward the Seebeck coefficient. In the case of D-I configuration, the energy difference between the light hole and heavy hole valence bands increases to ∼0.383 eV, further confirming that $Pb_9Sn_6MgTe_{16}$ has D-II configuration and not D-I.

Also, in order to compare the effect of Mg on $Pb_{10}Sn_6Te_{16}$ for the configuration reported earlier by Roychowdhury et al.,[10,11] the simulations were carried out with the same set of parameters as in the present work but with the configuration and supercell reported in the earlier papers. The electronic structure of $Pb_9Sn_6MgTe_{16}$ determined using $\sqrt{2} \times \sqrt{2} \times 2$ supercell reveals the opening up of band gap (∼0.046 eV), when the inversion symmetry is broken with the introduction of Mg into $Pb_{10}Sn_6Te_{16}$ crystal (Figure S2). This value is larger than that in the cases of Na (∼0.037 eV) and K (∼0.034 eV) doped samples.[10,11]

Optimizing the thermoelectric properties of bulk materials via doping largely depends on the solubility of the dopant in the parent matrix, hence increasing the solubility of the added dopant is highly essential.[1,24] In conventional solid solution alloying techniques like sealed tube melting reactions, the solubility is limited by equilibrium phase diagram, but in case of SHS higher solid solubility can be attained at room temperature by nonequilibrium process.[24,25] The intense heat released during the exothermic reaction makes the reaction self-propagating.[25] The method is rapid, facile, cost-effective, and scalable for large scale production. The obtained sample was subjected to powder processing and later densified in a graphite dye in vacuum using FAST technique, wherein a pulsed dc current directly passes through the dye. A temperature of 773 K was maintained outside the pressing tool system to minimize the thermal gradients, allowing enhanced heating rates at simultaneously optimized homogenity. The density of the pellets obtained (after cutting and polishing the ingots) was in the range ∼98% of the theoretical density.

$Pb_{0.6-x}Sn_{0.4}Mg_xTe$ (x = 0.0, 0.02, 0.04, 0.06, and 0.08) ingots were synthesized and characterized by pXRD. Figure 3a reveals that the diffraction pattern could be indexed to cubic NaCl structure with space group *Fm*3*m*. The formation of single phase was confirmed, as no other peaks of impurity were observed within the detection limits. Thus, SHS process can be successfully used for rapid preparation of single-phase materials with lower energy consumption and easier fabrication. The band gap of $Pb_{0.6-x}Sn_{0.4}Mg_xTe$ was resolved by using diffuse reflectance IR spectroscopy. The electronic absorption spectra showed a shift of absorption edge toward higher energy with increase in concentration of Mg up to 6 mol %. It is observed that the band gap increases from ∼0 to ∼0.4 eV while going from x = 0 to x = 0.06 in $Pb_{0.6-x}Sn_{0.4}Mg_xTe$ (Figure 3b). Replacement of Pb by Mg breaks the crystal mirror symmetry

DOI: 10.1021/acs.jpcc.7b07017
J. Phys. Chem. C 2017, 121, 20696−20703

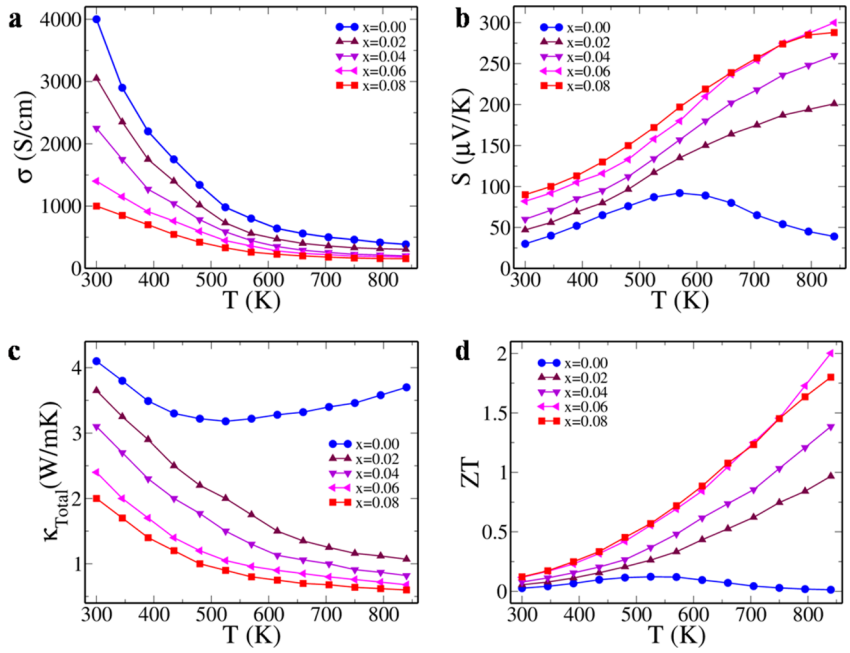

Figure 4. Thermoelectric properties of $Pb_{0.6-x}Sn_{0.4}Mg_xTe$. Variation of (a) electrical conductivity, (b) Seebeck coefficient, (c) total thermal conductivity, and (d) ZT with temperature.

locally and opens up the band gap as the protection of metallic states become void. Beyond 6 mol %, there is negligible change in the band gap (~0.405 eV for 8 mol %) suggesting the exclusion of dopant from the matrix, hence deviation from Vegards law.[12] This fact is further supported by the lattice constant measurements from XRD data. We know that the lattice constant of rock salt PbTe is ~6.46 Å, while that of SnTe is ~6.32 Å. Our experimental lattice constant for $Pb_{0.6-x}Sn_{0.4}Mg_xTe$ for $x = 0$ is ~6.408 Å, while for $x = 0.06$ is ~6.403 Å. Variation of lattice constant as a function of concentration of Mg is given in Figure 3c. The introduction of Sn into PbTe reduces the lattice parameter as size of Sn atom is smaller than Pb atom. Further introduction of Mg in place of Pb should have decreased the lattice constant largely as size of Mg is smaller compared to Pb. Here the observed difference is not much, further supporting the fact that Mg goes into zinc blende site. The lattice parameter of MgTe zinc blende form is ~6.45 Å, while rock salt structure is ~5.92 Å.[13] If Mg substituted Pb in the rock salt site, then we would have observed a further decrease in lattice constant with increase in Mg content. This result is in line with the theoretical results explained in previous section and is on par with the results of Mg−In codoped SnTe previously reported.[24] Beyond 6 mol % doping, we see negligible change in the lattice constant indicating the solubility limit to be 6 mol %. The experimental observation supported by theoretical study of occupation of zinc blende site by Mg may be an answer to solve the contradicting results observed by Ohta et al.[13] and Zhao et al.[12] for the lattice parameter variation with Mg content in PbTe and also the solubility limit of Mg in PbTe.

Thermoelectric transport properties as a function of temperature in the range of 300−840 K are shown in Figure 4. It is observed that the electrical conductivity values decrease with increase in concentration of Mg and with temperature throughout the range of measurement (Figure 4a). The decrease in the electrical conductivity with increase in temperature points to the degenerate semiconducting nature of the materials. However, in the case of Mg-doped samples, the electrical conductivity is lower compared to the pristine sample as opposed to the case of Na- and K-doped samples wherein the trend is reversed.[10−12,23] The room-temperature electrical conductivity decreases from 4000 S cm^{-1} to 1000 S cm^{-1} as x increases from 0 to 8 mol % in $Pb_{0.6-x}Sn_{0.4}Mg_xTe$. The carrier concentration is also seen to increase slightly from 9.51×10^{19} cm^{-3} to 1.7×10^{20} cm^{-3} as x increases from 0 to 8 mol %.

Figure 4b reveals that the Seebeck coefficients have positive values and show increasing trend with increase in temperature and Mg concentration. The positive value of Seebeck coefficient indicates the p-type conduction. The pristine sample shows a maximum value of Seebeck coefficient around 570 K, and there onward is a decrease in the value. This behavior clearly indicates the onset of bipolar diffusion. The intrinsic carriers get excited across the band gap, which adversely affects the Seebeck value because the minority carriers have Seebeck coefficients of opposite signs and hence will offset the effect of majority carriers.[1] Also, the contribution of minority carriers increases at higher temperatures.[12] In the case of Mg-doped samples, it is observed that the onset of bipolar diffusion shifts to higher temperature and goes beyond 840 K. The maximum Seebeck value of ~300 $\mu V K^{-1}$ achieved for $x = 0.06$ at 840 K is comparable to the Seebeck coefficient obtained in the case of MgTe-doped PbTe reported earlier.[12] This indicates the efficiency of the employed synthetic technique to produce samples with better transport properties with lesser lead content. For higher concentrations of Mg, Seebeck coefficient values did not decline with temperature in the temperature range studied here. This is due to the opening up of the band gap in the presence of Mg as band gap is directly proportional to the S_{max} and T_{max} apart from the fact that heavy doping causes an increase in the majority carriers which in turn suppress the bipolar effect.[12] The enhancement of Seebeck coefficient observed in the case of Mg-doped samples can also be attributed to the decrease in the energy separation between

DOI: 10.1021/acs.jpcc.7b07017
J. Phys. Chem. C 2017, 121, 20696−20703

the valence sub-bands causing the heavy hole band to contribute to a greater extent along with the light hole valence band and thus increasing the density of states effective mass (m^*), and in turn, the value of Seebeck coefficient as S is directly proportional to m^*. Hence, it is observed that with increase in the concentration of Mg doping the Seebeck coefficient also increases due to higher extent of convergence of the two valence sub-bands.[12,23]

Temperature dependence of the total thermal conductivity is as shown in Figure 4c. The thermal conductivity (total) contains contribution of lattice thermal conductivity, electronic thermal conductivity, and the bipolar thermal conductivities.[12] For $Pb_{0.6}Sn_{0.4}Te$ sample, the total thermal conductivity decreases initially, and beyond 525 K, it starts increasing.[10,11] The total thermal conductivity of the Mg-doped sample decreases with increase in percentage of doping as well as the temperature. The pristine sample shows very high contribution from bipolar thermal conductivity at higher temperatures as the material has almost zero band gap.[10,11] The bipolar component is due to the ambipolar diffusion of electrons and holes. At higher temperatures, the minority carriers not only decreases the value of Seebeck coefficient due to bipolar diffusion but also increases the thermal conductivity values as the diffusing electron hole pairs become an additional component. On the contrary, the contribution of bipolar thermal conductivity to the total thermal conductivity value decreases significantly as the concentration of Mg increases in the doped samples owing to opening up of the band gap and suppression of bipolar diffusion.

Usually the electronic thermal conductivity is determined using Wiedemann−Franz law (Electronic thermal conductivity = $L\sigma T$, where L is Lorenz number, σ is electrical conductivity, and T is absolute temperature). The lattice thermal conductivity in turn is determined by subtracting the electronic part from the total thermal conductivity,[23] but recent reports suggest that when multiple bands coexist at the Fermi level, the carriers move from one valley into another by means of a complex intervalley scattering.[24,25] This causes large amount of heat to transfer which cannot be determined by L value. In our present work, since there exists convergence of valence bands there is a possibility of intervalley scattering. Hence, we have not determined the lattice thermal conductivity, but it is safe to assume that the decrease in the total thermal conductivity with increase in doping concentration is due to two reasons: (i) decrease in the electronic component of total thermal conductivity caused due to decrease in electrical conductivity and (ii) decrease in lattice thermal conductivity due to the increase in the atomic point defects due to elemental substitution. The reduction in lattice thermal conductivity depends on the scattering parameter which is directly proportional to the doping fraction. The solid solution alloy of PbTe and SnTe has a lower thermal conductivity to begin with due to differences in atomic masses and radii of Pb and Sn which scatters the phonon. In addition to this, the added Mg dopant increases the scattering of the heat carrying phonons and hence causes further reduction in the lattice thermal conductivity.[1,2]

It is observed that the power factors obtained in the case of Mg-doped samples are higher compared to those of the pristine ones. The dependence of power factor on the temperature is shown in Figure S3. The increase in the value of Seebeck with the increase in Mg concentration is responsible for the increase in the power factor, but due to decrease in the electrical conductivity with increase in the concentration of Mg doping, the variation of power factor with temperature is not a smooth curve among the investigated compositions. The ZT value of $Pb_{0.6}Sn_{0.4}Te$ sample shows a gradual increase in value until 525 K (~0.12), and from there onward, it shows a decrease due to decrease in the power factor as well as the increase in the total thermal conductivity due to bipolar diffusion. The ZT values increased with an increase in Mg concentration (from x = 0.00 to x = 0.06), and a maximum ZT of ~2 at 840 K and ZT_{avg} (~1.2 between 500 and 840 K) were obtained for x = 0.06 in $Pb_{0.6-x}Sn_{0.4}Mg_xTe$ (Figure 4d). For x = 0.08, the ZT value decreases slightly to ~1.8, indicating x = 0.06 to be the optimum doping concentration. This ZT value of ~2 is the highest reported ZT value obtained for $Pb_{0.6-x}Sn_{0.4}M_xTe$ systems reported so far and is almost twice that of ZT obtained from doping monovalent group I elements.[10,11] The ZT_{avg} of ~1.2 is the highest reported average ZT among PbTe and SnTe class of materials to the best of our knowledge.[26] The ZT value is comparable to that of MgTe-doped PbTe (~2 at 823 K)[12] but is lower than that of SrTe-doped PbTe (~2.2 at 915 K, ~2.5 at 923 K)[15,16] and higher than those of MgTe-doped PbTe (~1.8 at 810 K, ~1.6 at 780 K),[13,14] HgTe-doped PbTe (~1.64 at 770 K),[17] CdTe-doped PbTe (~1.37 at 820 K),[17] CaTe-doped PbTe (~1.5 at 765 K),[18] and BaTe-doped PbTe (~1.3 at 760 K).[18] The ZT in the present work is also superior to those of Mg-doped SnTe (~1.2 at 856 K),[23] In-doped SnTe (~0.92 at 920 K),[25] HgTe-doped SnTe (~1.35 at 910 K),[27] CdTe-doped SnTe (~1.3 at 873 K),[28] CaTe-doped SnTe (~1.35 at 873 K),[29] MnTe-doped SnTe (~1.3 at 900 K, ~1.25 at 920 K),[30,31] and Ga-doped SnTe (~1 at 873 K).[32] The ZT in the present work for the singly Mg-doped sample is higher than those of Cd−In codoped SnTe (~1.4 at 923 K),[26] Ag−In codoped SnTe (~1 at 856 K),[33] Mg−In codoped SnTe (~1.5 at 840 K),[24] and Mg−In codoped $Sn_{0.7}Pb_{0.3}Te$ (~1 at 710 K).[34] These findings establish that doped $Pb_{0.6}Sn_{0.4}Te$ is a highly potential candidate for thermoelectric applications apart from giving scope for further investigation.

CONCLUSIONS

We have successfully demonstrated that doping of Mg can efficiently engineer the electronic structure and open up the band gap to render $Pb_{0.6}Sn_{0.4}Te$ into a high-performance thermoelectric material. In particular, the effect of Mg on $Pb_{0.6}Sn_{0.4}Te$ was studied both theoretically and experimentally. A combination of modified SHS and FAST technique was employed for the very first time in synthesis of solid solution of PbTe and SnTe. The most probable configuration of $Pb_{0.6}Sn_{0.4}Te$ was determined for the very first time using SOD technique. Both theoretical and experimental results show that Mg breaks the crystal mirror symmetry of $Pb_{0.6}Sn_{0.4}Te$ and opens up the band gap. This causes suppression of bipolar thermal conduction. Also, the presence of Mg decreases the energy separation between light- and heavy-hole valence sub-bands. Thus, an increase in contribution of heavy-hole valence band due to increase in valence band degeneracy causes improvement in the Seebeck coefficient. Both these synergistic effects lead to remarkable improvement in the ZT (~2 at 840 K) and ZT_{avg} (~1.2 between 500 and 840 K) of the Mg-alloyed $Pb_{0.6}Sn_{0.4}Te$. This value of average ZT is highest one for this class of materials by far. The results indicate that chemical doping using group II elements can remarkably improve the ZT of $Pb_{0.6}Sn_{0.4}Te$ and opens a new avenue to create thermo-

DOI: 10.1021/acs.jpcc.7b07017
J. Phys. Chem. C 2017, 121, 20696−20703

electric materials with high ZT using chemical doping with elements which can behave similar to Mg.

■ ASSOCIATED CONTENT

Supporting Information

The Supporting Information is available free of charge on the ACS Publications website at DOI: 10.1021/acs.jpcc.7b07017.

Electronic structure of $Pb_9Sn_6MgTe_{16}$ (D-II configuration) with Mg in zinc blende site determined using a $2 \times 2 \times 1$ supercell, crystal structures and electronic structures of $Pb_{10}Sn_6Te_{16}$ and $Pb_9Sn_6MgTe_{16}$ determined using a $\sqrt{2} \times \sqrt{2} \times 2$ supercell, temperature-dependent power factor of $Pb_{0.6-x}Sn_{0.4}Mg_xTe$ (x = 0.0−0.08) (PDF)

■ AUTHOR INFORMATION

Corresponding Author

*E-mail: denthajekb@gmail.com.

ORCID

D. Krishna Bhat: 0000-0003-0383-6017

Notes

The authors declare no competing financial interest.

■ ACKNOWLEDGMENTS

We gratefully acknowledge SERB and CSIR, Government of India for financial support in the form of R&D project grants.

■ REFERENCES

(1) Tan, G.; Zhao, L. D.; Kanatzidis, M. G. Rationally designing high-performance bulk thermoelectric materials. *Chem. Rev.* **2016**, *116*, 12123−12149.

(2) Snyder, G. J.; Toberer, E. S. Complex thermoelectric materials. *Nat. Mater.* **2008**, *7*, 105−114.

(3) Xu, S. Y.; Liu, C.; Alidoust, N.; Neupane, M.; Qian, D.; Belopolski, I.; Denlinger, J. D.; Wang, Y. J.; Lin, H.; Wray, L. A.; et al. Observation of a topological crystalline insulator phase and topological phase transition in $Pb_{1-x}Sn_xTe$. *Nat. Commun.* **2012**, *3*, 1192.

(4) Mitrofanov, K. V.; Kolobov, A. V.; Fons, P.; Krbal, M.; Tominaga, J.; Uruga, T. Study of band inversion in the $Pb_{1-x}Sn_xTe$ class of topological crystalline insulators using X-ray absorption spectroscopy. *J. Phys.: Condens. Matter* **2014**, *26*, 475502.

(5) Saghir, M.; Sanchez, A. M.; Hindmarsh, S. A.; York, S. J.; Balakrishnan, G. Nanomaterials of the topological crystalline insulators, $Pb_{1-x}Sn_xTe$ and $Pb_{1-x}Sn_xSe$. *Cryst. Growth Des.* **2015**, *15*, 5202−5206.

(6) Arachchige, I. U.; Kanatzidis, M. G. Anomalous band gap evolution from band inversion in $Pb_{1-x}Sn_xTe$ nanocrystals. *Nano Lett.* **2009**, *9*, 1583−1587.

(7) Liu, J.; Hsieh, T. H.; Wei, P.; Duan, W.; Moodera, J.; Fu, L. Spin-filtered edge states with an electrically tunable gap in a two-dimensional topological crystalline insulator. *Nat. Mater.* **2013**, *13*, 178.

(8) Serbyn, M.; Fu, L. Symmetry breaking and Landau quantization in topological crystalline insulators. *Phys. Rev. B: Condens. Matter Mater. Phys.* **2014**, *90*, 035402.

(9) Liu, J.; Qian, X.; Fu, L. Crystal field effect induced topological crystalline insulators in monolayer IV-VI semiconductors. *Nano Lett.* **2015**, *15*, 2657−2661.

(10) Roychowdhury, S.; Shenoy, U. S.; Waghmare, U. V.; Biswas, K. Tailoring of electronic structure and thermoelectric properties of a topological crystalline insulator by chemical doping. *Angew. Chem., Int. Ed.* **2015**, *54*, 15241−15245.

(11) Roychowdhury, S.; Shenoy, U. S.; Waghmare, U. V.; Biswas, K. Effect of potassium doping on electronic structure and thermoelectric properties of topological crystalline insulator. *Appl. Phys. Lett.* **2016**, *108*, 193901.

(12) Zhao, L. D.; Wu, H. J.; Hao, S. Q.; Wu, C. I.; Zhou, X. Y.; Biswas, K.; He, J. Q.; Hogan, T. P.; Uher, C.; Wolverton, C.; et al. All-scale hierarchical thermoelectrics: MgTe in PbTe facilitates valence band convergence and suppresses bipolar thermal transport for high performance. *Energy Environ. Sci.* **2013**, *6*, 3346−3355.

(13) Ohta, M.; Biswas, K.; Lo, S. H.; He, J.; Chung, D. Y.; Dravid, V. P.; Kanatzidis, M. G. Enhancement of thermoelectric figure of merit by the insertion of MgTe nanostructures in p-type PbTe doped with Na_2Te. *Adv. Energy Mater.* **2012**, *2*, 1117−1123.

(14) Hu, X.; Jood, P.; Ohta, M.; Kunii, M.; Nagase, K.; Nishiate, H.; Kanatzidis, M. G.; Yamamoto, A. Power generation from nanostructured PbTe-based thermoelectrics: comprehensive development from materials to modules. *Energy Environ. Sci.* **2016**, *9*, 517−529.

(15) Biswas, K.; He, J.; Blum, I. D.; Wu, C. I.; Hogan, T. P.; Seidman, D. N.; Dravid, V. P.; Kanatzidis, M. G. High-performance bulk thermoelectrics with all-scale hierarchical architectures. *Nature* **2012**, *489*, 414−418.

(16) Tan, G.; Shi, F.; Hao, S.; Zhao, L. D.; Chi, H.; Zhang, X.; Uher, C.; Wolverton, C.; Dravid, V. P.; Kanatzidis, M. G. Non-equilibrium processing leads to record high thermoelectric figure of merit in PbTe-SrTe. *Nat. Commun.* **2016**, *7*, 12167.

(17) Ahn, K.; Biswas, K.; He, J.; Chung, I.; Dravid, V.; Kanatzidis, M. G. Enhanced thermoelectric properties of p-type nanostructured PbTe-MTe (M= Cd, Hg) materials. *Energy Environ. Sci.* **2013**, *6*, 1529−1537.

(18) Biswas, K.; He, J.; Wang, G.; Lo, S. H.; Uher, C.; Dravid, V. P.; Kanatzidis, M. G. High thermoelectric figure of merit in nanostructured p-type PbTe-MTe (M = Ca, Ba). *Energy Environ. Sci.* **2011**, *4*, 4675−4684.

(19) Rogers, L. M. Valence band structure of SnTe. *J. Phys. D: Appl. Phys.* **1968**, *1*, 845.

(20) Grau-Crespo, R.; Hamad, S.; Catlow, C. R. A.; de Leeuw, N. H. Symmetry-adapted configurational modeling of fractional site occupancy in solids. *J. Phys.: Condens. Matter* **2007**, *19*, 256201.

(21) Giannozzi, P.; Baroni, S.; Bonini, N.; Calandra, M.; Car, R.; Cavazzoni, C.; Ceresoli, D.; Chiarotti, G. L.; Cococcioni, M.; Dabo, I.; et al. Quantum espresso: a modular and open-source software project for quantumsimulations of materials. *J. Phys.: Condens. Matter* **2009**, *21*, 395502.

(22) Perdew, J. P.; Burke, K.; Ernzerhof, M. Generalized gradient approximation made simple. *Phys. Rev. Lett.* **1996**, *77*, 3865−3868.

(23) Banik, A.; Shenoy, U. S.; Anand, S.; Waghmare, U. V.; Biswas, K. Mg alloying in SnTe facilitates valence band convergence and optimizes thermoelectric properties. *Chem. Mater.* **2015**, *27*, 581−587.

(24) Bhat, D. K.; Shenoy, U. S. High thermoelectric performance of co-doped tin telluride due to synergistic effect of magnesium and indium. *J. Phys. Chem. C* **2017**, *121*, 7123−7130.

(25) Liang, T.; Su, X.; Tan, X.; Zheng, G.; She, X.; Yan, Y.; Tang, X.; Uher, C. Ultra-fast non-equilibrium synthesis and phase segregation in $In_xSn_{1-x}Te$ Thermoelectrics by SHS-PAS Processing. *J. Mater. Chem. C* **2015**, *3*, 8550−8558.

(26) Tan, G.; Shi, F.; Hao, S.; Chi, H.; Zhao, L. D.; Uher, C.; Wolverton, C.; Dravid, V. P.; Kanatzidis, M. G. Codoping in SnTe: enhancement of thermoelectric performance through synergy of resonance levels and band convergence. *J. Am. Chem. Soc.* **2015**, *137*, 5100−5112.

(27) Tan, G.; Shi, F.; Doak, J. W.; Sun, H.; Zhao, L. D.; Wang, P.; Uher, C.; Wolverton, C.; Dravid, V. P.; Kanatzidis, M. G. Extraordinary role of Hg in enhancing the thermoelectric performance of p-type SnTe. *Energy Environ. Sci.* **2015**, *8*, 267−277.

(28) Tan, G.; Zhao, L. D.; Shi, F.; Doak, J. W.; Lo, S. H.; Sun, H.; Wolverton, C.; Dravid, V. P.; Uher, C.; Kanatzidis, M. G. High thermoelectric performance of p-type SnTe via a synergistic band engineering and nanostructuring approach. *J. Am. Chem. Soc.* **2014**, *136*, 7006−7017.

(29) Al Rahal Al Orabi, R.; Mecholsky, N. A.; Hwang, J.; Kim, W.; Rhyee, J. S.; Wee, D.; Fornari, M. Band Degeneracy, low thermal conductivity, and high thermoelectric figure of merit in SnTe-CaTe alloys. *Chem. Mater.* **2016**, *28*, 376−384.

(30) Tan, G.; Shi, F.; Hao, S.; Chi, H.; Bailey, T. P.; Zhao, L. D.; Uher, C.; Wolverton, C.; Dravid, V. P.; Kanatzidis, M. G. Valence band modification and high thermoelectric performance in SnTe heavily alloyed with MnTe. *J. Am. Chem. Soc.* **2015**, *137*, 11507−11516.
(31) He, J.; Tan, X.; Xu, J.; Liu, G. Q.; Shao, H.; Fu, Y.; Wang, X.; Liu, Z.; Xu, J.; Jiang, H.; Jiang, J. Valence band engineering and thermoelectric performance optimization in SnTe by Mn-alloying via a zone melting method. *J. Mater. Chem. A* **2015**, *3*, 19974−19979.
(32) Al Rahal Al Orabi, R.; Hwang, J.; Lin, C. C.; Gautier, R.; Fontaine, B.; Kim, W.; Rhyee, J. S.; Wee, D.; Fornari, M. Ultra-low lattice thermal conductivity and enhanced thermoelectric performance in SnTe:Ga materials. *Chem. Mater.* **2017**, *29*, 612−620.
(33) Banik, A.; Shenoy, U. S.; Saha, S.; Waghmare, U. V.; Biswas, K. High power factor and enhanced thermoelectric performance of SnTe-$AgInTe_2$: synergistic effect of resonance level and valence band convergence. *J. Am. Chem. Soc.* **2016**, *138*, 13068−13075.
(34) Roychowdhury, S.; Shenoy, U. S.; Waghmare, U. V.; Biswas, K. An enhanced Seebeck coefficient and high thermoelectric performance in p-type In and Mg co-doped Sn1−*x*PbxTe via the co-adjuvant effect of the resonance level and heavy hole valence band. *J. Mater. Chem. C* **2017**, *5*, 5737.

DOI: 10.1021/acs.jpcc.7b07017
J. Phys. Chem. C 2017, 121, 20696−20703